Molecular kinetic modelling of nano-scale slip flow using a continuum approach

Molecular kinetic modelling of nano-scale slip flow using a continuum approach

Baochao Shan[1], Peng Wang [1], Runxi Wang [2], Yonghao Zhang[2]†, and Zhaoli Guo[1]‡

[1]State Key Laboratory of Coal Combustion, Huazhong University of Science and Technology, Wuhan 430074, China

[2]School of Engineering, The University of Edinburgh, Edinburgh EH9 3FB, UK

(Received xx; revised xx; accepted xx)

One major challenge for a continuum model to describe nano-scale confined fluid flows is the lack of a boundary condition that can capture molecular-scale slip behaviours. In this work, we propose a molecular-kinetic boundary condition to model the fluid-surface and fluid-fluid molecular interactions using the Lennard-Jones type potentials, and add a mean-field force to the momentum equation. This new boundary condition is then applied to investigate the nanoscale Couette and Poiseuille flows using the generalised hydrodynamic model developed by Guo *et al.* (2006*a*). The accuracy of our model is validated by molecular dynamics simulations and other models for a broad range of parameters including density, shear rate, wettability and channel width. Our simulation results reveal some unexpected and unintuitive slip behaviours at the nanoscale, including the epitaxial layering structure of fluids and the slip length minimum. The slip length minimum, which is analogous to the Knudsen minimum, can be explained by competing fluid-solid and fluid-fluid molecular interactions as density varies. A new scaling law is proposed for the slip length to account for not only the competing effect between the fluid-solid and fluid-fluid molecular interactions, but also many other physical mechanisms including the competition between the fluid internal potential energy and kinetic energy, and the confinement effect. While the slip length is nearly constant at the low shear rates, it increases rapidly at the high shear rates due to friction reduction. These molecular-scale slip behaviours are caused by energy corrugations at the fluid-solid interface where strong fluid-solid and fluid-fluid molecular interactions interplay.

Key words: Molecular kinetic theory, gas kinetic theory, slip length, slip dynamics, nanoflow

1. Introduction

Although the no-slip boundary condition is widely adopted in continuum fluid dynamics, it fails to account for the unexpected fast mass transport of fluids in the nanoscale systems (Holt *et al.* 2006; Falk *et al.* 2010; Secchi *et al.* 2016), and may even lead to unrealistic simulated

† Email address for correspondence: yonghao.zhang@ed.ac.uk
‡ Email address for correspondence: zlguo@hust.edu.cn

flow behaviours in, e.g. a liquid spreading on a solid substrate, corner flows, and extrusion of polymer melts from a capillary tube (Thompson & Troian 1997). In recent years, the rapid development of micro/nano technologies and related industrial processes including shale gas extraction, gas separation, self-cleaning surfaces, and tribology and lubrication (Wu *et al.* 2016; Cai *et al.* 2019; Sholl & Johnson 2006; Yao *et al.* 2015; Urbakh *et al.* 2004; Ma *et al.* 2015; Ho *et al.* 2019a) poses a research challenge in understanding and quantifying fluid slip dynamics at a fluid-solid interface, which may help to develop energy-efficient transportation with significant drag-reduction (Martini *et al.* 2008*a*).

Slip dynamics of fluids over a solid surface has been extensively studied experimentally (Zhu & Granick 2001; Secchi *et al.* 2016; Henot *et al.* 2018), theoretically (Richardson 1973; Lauga & Stone 2003; Nott 2011; Wu *et al.* 2017; Zampogna *et al.* 2018; Wang & Hadjiconstantinou 2019), and numerically (Thompson & Troian 1997; Sholl & Johnson 2006; Martini *et al.* 2008*a*,*b*; Falk *et al.* 2010; Bailey *et al.* 2017; Ho *et al.* 2020). Due to difficulties and limitations of experimental and theoretical studies, molecular dynamics (MD) simulations have been widely adopted to probe the microscopic slip behaviours of fluids at the fluid-solid interface (Thompson & Troian 1997; Hsu & Patankar 2010). MD results show that surface effect is prominent in nanofluidics, and molecular-scale slip behaviours are greatly affected by the wall molecular potentials (Guo *et al.* 2006*a*; Mashayak & Aluru 2012), the cross-sectional fluid density and viscosity oscillations (Bhadauria *et al.* 2015; Heiranian & Aluru 2020), and the fluid molecular interactions (Thompson & Troian 1997; Martini *et al.* 2008*a*,*b*; Ho *et al.* 2011; Bitrián & Principe 2018). These valuable insights help to understand the mechanisms of molecular-scale slips at a fluid-solid interface from the molecular perspective. Due to the computational cost, MD simulations are restricted to extremely small systems and time steps, which has motivated researchers to develop computationally more efficient methods, e.g. continuum models. However, to date, it remains an open question on how to capture these molecular characteristics in a continuum modelling framework.

The difficulties of a continuum model in reproducing molecular-scale slip behaviours are mainly caused by inhomogeneities of the fluids with a vast fluid/surface region in nanoscale systems (Richardson 1973; Hocking 1976; Priezjev & Troian 2006), where the fluid properties and its dynamical behaviour are significantly different from the bulk region (Sochi 2011; Guo *et al.* 2006*a*; Mashayak & Aluru 2012; Bhadauria *et al.* 2015). For example, the epitaxial layering structure of fluids near the wall surface of a nano-confined system is associated with the molecular-scale slip at the fluid-solid interface (Voronov *et al.* 2008), which can dramatically change the momentum transfer efficiency between the fluid and solid surface (Cao *et al.* 2006). Consequently, in order to reproduce molecular-scale slip behaviours by a continuum model, it is imperative to take these molecular-scale characteristics into account in a continuum modelling approach (Hsu & Patankar 2010; Bhadauria *et al.* 2015; Heiranian & Aluru 2020).

In recent years, some attempts have been made to develop continuum models to investigate molecular-scale slip behaviours in a nanoscale system (Hsu & Patankar 2010) where the continuum fluid mechanics meets the molecular nature of matters (Secchi *et al.* 2016). For example, Hsu & Patankar (2010) studied the molecular-scale slip behaviours in the nano-channels, which indicates that the continuum approach can describe molecular-scale slip behaviours provided underlying molecular-scale physics can be properly considered. According to Hsu & Patankar (2010), the following two challenges remain to be tackled.

(i) An effective solid-fluid potential, consistent with MD simulations, is needed to accurately describe surface fluid interactions.

(ii) The molecular interactions between fluid molecules require to consider the non-ideal gas effect in a dense fluid.

The generalised hydrodynamic model developed previously by one of the authors has partly addressed the second challenge (Guo *et al.* 2006*a*), where the Enskog equation for dense gases was used to take account of non-ideal gas effect, and considered the surface-fluid interactions through the Lennard-Jones (LJ) type potentials, which has shown to be able to predict fluid layering structure in nano-confined spaces (Guo *et al.* 2006*b*; Shan *et al.* 2020). While these works indicate the feasibility of the continuum approach, the molecular-scale slip behaviours at the surface are not encapsulated, which will be addressed in the present work.

The molecular kinetic theory (MKT) has been proved to be effective in modelling chemical reactions (Glasstone *et al.* 1941), viscous flow (Martini *et al.* 2008*a*; Wang & Zhao 2011; Wang & Hadjiconstantinou 2019), and wetting dynamics (De Coninck & Blake 2008; Yuan & Zhao 2013), which bridges the molecular and continuum scales. While progress has been made to understand slip dynamics at the nanoscale, the underlying slip mechanisms are not fully understood. A slip model for a predictive simulation tool which encapsulates essential slip physics in particular fluid molecular interaction is still lacking (Wang & Hadjiconstantinou 2019).

Here, a new MKT slip model will be developed to consider the effect of molecular interactions between the fluid molecules and between the fluid/solid molecules on slip dynamics at the nano-scale. Together with the generalised hydrodynamic model (Guo *et al.* 2006*a*), the fluid dynamics at the nanometer scale can be described by a continuum approach. In § 2, a brief introduction to the generalised hydrodynamic model and slip dynamics at the nano-scale is given. In § 3, the molecular-scale slip dynamics in strongly inhomogeneous nano-scale system is discussed, leading to the new molecular-kinetic boundary condition. The simulation details and discussions are presented in § 4, and the conclusions are given in § 5.

2. Governing equation and molecular-scale slip

Here, we will use a continuum model to describe slip behaviour of fluid flows in confined nano-scale spaces. At the nanometer scale, the van der Waals forces between fluid molecules and between fluid-solid molecules become important, which are normally ignored in a continuum model. The fluid properties including density and viscosity oscillate significantly over a molecule size due to the fluid-solid and fluid-fluid molecular interactions (Bitsanis *et al.* 1988; Bhadauria *et al.* 2015; Heiranian & Aluru 2020). Therefore, such a system at the nano-scale is strongly inhomogeneous (Davis 1987; Bitsanis *et al.* 1988; Vanderlick *et al.* 1989; Pozhar & Gubbins 1993; Guo *et al.* 2006*b*; Dalton *et al.* 2015; Shan *et al.* 2020). As shown in figure 1 (*a*) and (*b*), a depletion area exists in the immediate vicinity of the wall due to the volume exclusion effect or the short-range repulsion between solid and fluid molecules, which leads to difference between the physical boundary and the slip plane (Bhadauria *et al.* 2015).

According to the fluid density distribution across the channel, the fluid can be divided into an interfacial region near the wall and a bulk region in the center as shown in figure 1 (*a*). The interfacial region arises due to competing solid-fluid and fluid molecular interactions, exhibiting a layering structure near the wall (Patashinski *et al.* 2019; Kavokine *et al.* 2021). Consequently, the interfacial region is also called gas adsorption area or adsorption layers, where the fluid density is normally larger than bulk density due to usually strong solid-fluid molecular attractions near the wall. In the bulk region, fluid molecules would not be affected by the wall potential, so the fluid density is constant.

Generally, the conventional Navier-Stokes (NS) equation, which describes fluid flows in a homogeneous system, will not be applicable to the interfacial region of strongly

inhomogeneous fluids. In this work, we attempt to model nano-scale flows using a continuum approach, focusing on simple fluids.

2.1. *Generalised hydrodynamic model*

To reproduce molecular-scale slip behaviours by a continuum model, the fluid-solid and fluid molecular interactions should be appropriately taken into account (Hsu & Patankar 2010). As an extension of the NS equation, a generalised hydrodynamic model was proposed by Guo *et al.* (2006*a*) based on the gas kinetic theory, which is applicable to both homogeneous and inhomogeneous systems. The mass and momentum conservation equations in this generalised hydrodynamic model can be written as

$$\partial_t \rho + \boldsymbol{\nabla} \cdot (\rho \boldsymbol{u}) = 0, \tag{2.1a}$$

$$\partial_t (\rho \boldsymbol{u}) + \boldsymbol{\nabla} \cdot (\rho \boldsymbol{u}\boldsymbol{u}) + RT\boldsymbol{\nabla}\rho + \frac{\rho}{m}[\boldsymbol{\nabla}(\phi_w + \phi_m) - \boldsymbol{G}] = \boldsymbol{\nabla} \cdot \left(\eta \widetilde{\boldsymbol{\nabla} \boldsymbol{u}}\right) - \rho RT\,(2\boldsymbol{A}\chi + \boldsymbol{B}\overline{n})\,V_0, \tag{2.1b}$$

where $\rho = mn$ is the fluid density with m being the mass of a fluid molecule and n being the fluid number density, i.e. the fluid molecule numbers per unit volume; u, the fluid velocity; t, the time; ϕ_w and ϕ_m, the wall potential and the fluid potential related to intermolecular attractions, respectively; $\boldsymbol{G}$, the body force; η, the fluid viscosity; $R = k_B/m$, the gas constant with k_B being the Boltzmann constant; T, the fluid temperature; χ, the radial distribution function; $V_0 = 2\pi\sigma^3/3$; $\overline{n}$, the local average density (Bitsanis *et al.* 1987); $\widetilde{\boldsymbol{\nabla} \boldsymbol{u}} = \boldsymbol{\nabla} \boldsymbol{u} + (\boldsymbol{\nabla} \boldsymbol{u})^{\intercal}$; and $\boldsymbol{A}$ and $\boldsymbol{B}$, the two vector functions defined by (Guo *et al.* 2005)

$$\boldsymbol{A}(\boldsymbol{r}) = \frac{1}{D}\int_{|\boldsymbol{r}'|<\sigma/2} \boldsymbol{r}'\overline{n}(\boldsymbol{r} + \boldsymbol{r}')\,\mathrm{d}\boldsymbol{r}', \tag{2.2a}$$

$$\boldsymbol{B}(\boldsymbol{r}) = \frac{1}{D}\int_{|\boldsymbol{r}'|<\sigma/2} \boldsymbol{r}'\chi[\overline{n}(\boldsymbol{r} + \boldsymbol{r}')]\,\mathrm{d}\boldsymbol{r}', \tag{2.2b}$$

where $D = \pi\sigma^5/120$ with σ being the fluid molecule diameter, and $\boldsymbol{r}$ is the spatial position.

According to the Enskog theory for dense fluids (Chapman & Cowling 1970), fluid viscosity needs to be corrected for dense fluids as fluid molecule size is not negligible and collisional transfer of momentum and energy needs to be considered, which can be evaluated by

$$\eta = \eta_0 \overline{n}_f V_0 [(\overline{n}_f V_0 \chi)^{-1} + 0.8 + 0.7614 \overline{n}_f V_0 \chi], \tag{2.3}$$

where η_0 is the fluid viscosity for a dilute gas.

For a two-dimensional flow as shown in figure 1(*b*), equation (2.1*b*) in the y-direction reduces to

$$\frac{d}{dy}\left(\ln n_f + \frac{\phi_w + \phi_m}{k_B T}\right) = -(2A\chi + B\overline{n}_f)V_0, \tag{2.4}$$

from which the density distribution across the channel can be obtained.

For Couette and Poiseuille flows, the velocity component in the x-direction can be determined by

$$\frac{d}{dy}\left(\eta \frac{du}{dy}\right) = 0, \tag{2.5}$$

and

$$\frac{d}{dy}\left(\eta \frac{du}{dy}\right) + G_x n = 0, \tag{2.6}$$

respectively, with G_x in (2.6) being a constant external force in the flow direction.

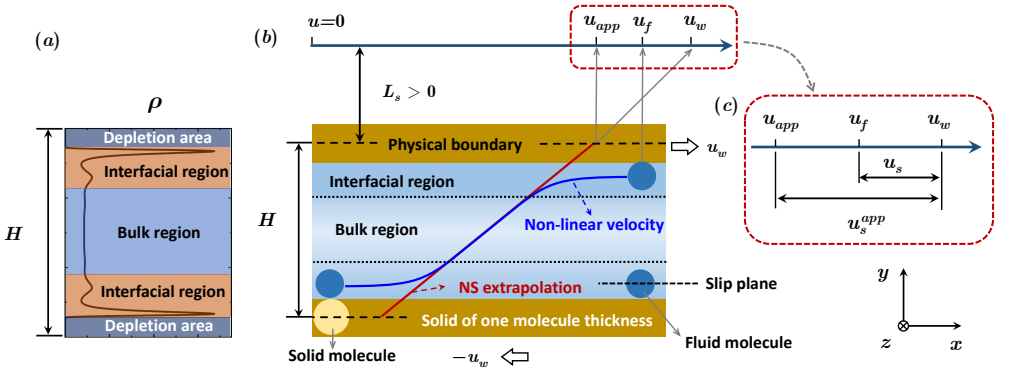

Figure 1: Schematic of a nano-scale Couette flow and illustration of molecular-scale slip at the surface: (a) division of flow regions according to the density distribution; (b) the true and extrapolated velocity of a Couette flow; (c) the relationship between the micro and apparent velocities.

As we can see from (2.4), (2.5) and (2.6), both density and velocity profiles are position-dependent in nano-confined channels due to the effects of wall potential and fluid molecular interactions. This position-dependence of fluid properties lead to some interesting and unexpected flow behaviours. However, in order to solve (2.5) and (2.6), appropriate boundary conditions, which are currently lacking, need to be specified.

2.2. *Molecular scale slip*

As discussed above, some unique features exist in strongly inhomogeneous fluid flows: (i) there is an interfacial region (also called an adsorption layer) near the wall, where the fluid density is much higher than in the bulk region, while the cross-sectional density is uniform in a conventional homogeneous system; (ii) in addition to the density and viscosity oscillations, the shear rate of a Couette flow is no longer constant and the velocity distribution is not linear, see figure 1. Similarly, the shear rate in a Poiseuille flow is no longer linear, with the velocity distribution being non-parabola; (iii) due to the finite size of fluid and solid molecules, and the strong repulsion between them when they are close, the first fluid layer is away from the physical boundary, i.e. the solid surface, which is illustrated by the dashed lines in figure 1(b). These molecular features affect dynamics of strongly inhomogeneous fluid including both the velocity slip at the fluid-solid interface and the velocity distribution across the channel.

The slip phenomenon is generally quantified by the slip length L_s (Thompson & Troian 1997; Martini *et al.* 2008*a*; Hsu & Patankar 2010; Wang & Hadjiconstantinou 2019), which can be calculated according to the Navier slip boundary condition

$$L_s = \frac{u_s^{app}}{\gamma}, \tag{2.7}$$

where u_s^{app} is the apparent slip velocity as shown in figure 1(c), and γ is the shear rate evaluated in the bulk region. This is to say, the slip length in (2.7) is associated with the bulk region properties, where the NS equation is assumed to be valid. As shown in figure 1(b), a slip length is positive when the extrapolated position, where the extrapolated velocity becomes equal to the wall velocity, is outside the physical boundary. And the slip is also called a positive slip. Otherwise, it is a negative or stick slip. Not only does the velocity distribution depend on fluid information in the bulk region (*e.g.* viscosity), but also the molecular interactions in the interfacial region (*e.g.* the fluid layering structure).

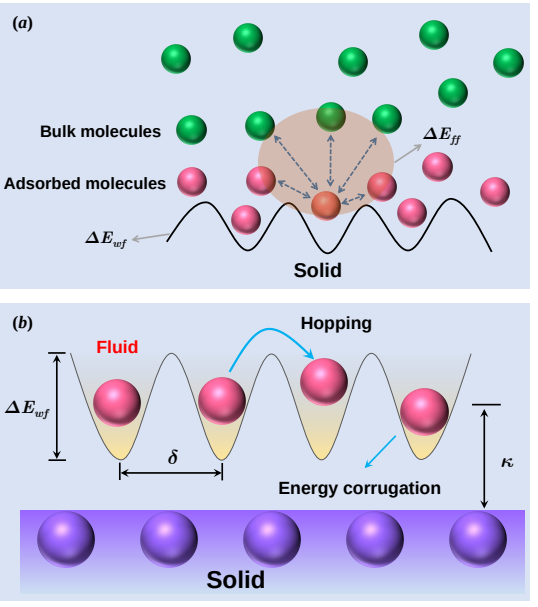

Figure 2: The schematic of fluid molecules passing over a solid surface. (a) The total resistance from the fluid-solid interaction ΔE_{wf} and fluid-fluid molecular interaction ΔE_{ff}. (b) The lattice structure of a solid wall and the related energy corrugations over the surface.

Taking a Couette flow as an example, in order to obtain the velocity distribution across the whole channel which is non-linear as shown in figure 1(b), the fluid velocity at the boundary needs to be determined. For strongly inhomogeneous nano-scale flows, a velocity difference exists between the wall and the fluid at the wall due to slip, which is called micro slip velocity $u_s = |u_w - u_f|$, as shown in figure 1(c). While the apparent slip velocity u_s^{app} can be close to the true slip velocity u_s when the interfacial region is negligible, their difference can be significant when the characteristic length of the flow domain reduces to the nano-scale. Therefore, we need to determine the true slip velocity u_s to obtain the velocity distribution of strongly inhomogeneous flows.

3. Slip mechanisms and molecular kinetic modelling

In the previous slip models that are based on MKT, the slip resistance is usually considered to be caused by the fluid-solid molecular interaction only, e.g. (Glasstone *et al.* 1941; Wang & Zhao 2011). However, fluid molecular interaction was found to contribute to slip resistance in nanoscale flows, which should be considered properly in a MKT slip model. (Wang & Hadjiconstantinou 2019).

3.1. *Slip mechanisms and related models*

The slip dynamics of strongly inhomogeneous flows at the solid-liquid interface can be modelled as a thermally activated process (Glasstone *et al.* 1941; Lichter *et al.* 2007; Wang & Zhao 2011; Wang & Hadjiconstantinou 2019). Two key factors in MKT are the hopping length δ and the hopping rate α. At equilibrium, fluid molecules preferentially occupy the most stable vacancies in energy corrugations. The hopping rates for the fluid molecules to move forwards and backwards are equal, which follows the Arrhenius dynamics (Glasstone

et al. 1941; Martini *et al.* 2008*b*) as

$$\alpha_+ = \alpha_- = \alpha_0 = \frac{k_B T}{h}\exp\left(-\frac{\Delta E}{k_B T}\right), \tag{3.1}$$

where α_+, α_- and α_0 are the hopping rates of moving forwards, backwards and at equilibrium, respectively; h is the Planck constant; ΔE is the total energy barrier depth, which represents the total slip resistance from fluid-fluid and fluid-solid molecular interactions.

If a shear stress τ is exerted on fluid molecules in the flow direction, the energy of a fluid molecule to move forwards is elevated by the magnitude of $0.5\tau S\delta$, where S is the effective area that the fluid molecule experiences the shear, so the probability of the fluid molecules to move forwards and backwards can be expressed by

$$\alpha_+ = \frac{k_B T}{h}\exp\left(-\frac{\Delta E - 0.5\tau S\delta}{k_B T}\right), \tag{3.2a}$$

$$\alpha_- = \frac{k_B T}{h}\exp\left(-\frac{\Delta E + 0.5\tau S\delta}{k_B T}\right). \tag{3.2b}$$

The slip velocity $u_s = \delta(\alpha_+ - \alpha_-)$ can consequently be calculated by

$$u_s = \delta\frac{2k_B T}{h}\exp\left(-\frac{\Delta E}{k_B T}\right)\sinh\left(\frac{\tau S\delta}{2k_B T}\right). \tag{3.3}$$

This is the classic MKT slip model proposed by Glasstone *et al.* (1941).

Based on the slip model (3.3), many other MKT models have been proposed to extend its applicability. Yang (2020) took the critical shear stress into account and proposed a new slip model. Similarly, Wang & Zhao (2011) considered both the critical shear stress and the energy dissipation near the liquid-solid interface, and proposed the following extended MKT slip model

$$u_s = f_d\delta\frac{2k_B T}{h}\frac{F^+}{F_0}\exp\left(-\frac{E_0}{k_B T}\right)\sinh\left[\frac{\mathrm{Hev}(\tau - \tau_c)S\delta}{2k_B T}\right], \tag{3.4}$$

where E_0 is the activation energy at the absolute zero, f_d is a dissipation factor, accounting for the energy dissipation between liquid layers at high shear stress, which is unity at low and moderate shear stress; and Hev() is the Heaviside function.

The critical shear stress τ_c was conjectured from experiments (Granick *et al.* 2003), but was found to be negligible in numerical simulations (Ma *et al.* 2011). In the linear flow regime, the energy dissipation factor f_d may be neglected, so the slip model (3.4) reduces to (3.3). The above models (3.3) and (3.4) only consider the effect of fluid-solid molecular interaction on the slip resistance, and ignor the fluid molecular interaction.

3.2. *Effect of fluid molecular interactions on slip dynamics*

According to Blake & De Coninck (2002) and Zhao & Cheng (2017), the total resistance in a rate process arises from both fluid-solid and fluid-fluid molecular interactions, as shown in figure 2(*a*). Assuming the superposition of the both potential contributions (Blake & De Coninck 2002; Wang & Hadjiconstantinou 2019), i.e.

$$\Delta E = \Delta E_{wf} + \Delta E_{ff}, \tag{3.5}$$

where ΔE_{wf} and ΔE_{ff} are the energy barrier depths related to fluid-solid and fluid-fluid molecular interactions, respectively, Wang & Hadjiconstantinou (2019) proposed the

following slip model

$$u_s = 2\delta\omega_0 \exp\left(-\frac{\Delta E_{wf}}{k_B T}\right) \sinh\left(\frac{S\delta}{2k_B T}\eta\gamma\right). \tag{3.6}$$

In (3.6), the shear stress τ in (3.3) is replaced by the product of viscosity η and shear rate γ, which are evaluated at the interface between the interfacial and bulk regions. The slip length dependency on density, temperature and fluid-solid coupling strength has been fully investigated by Wang & Hadjiconstantinou (2019). However, the parameter δ and the term $\omega_0 \exp\left[-\Delta E_{wf}/(k_B T)\right]$ are treated as fitting parameters which need to be calibrated for every operation condition by MD or experimental data. Therefore, this model provides a way to post-process MD or experimental data and does not have predictive power.

3.3. *Molecular kinetic modelling and analysis*

Although the slip resistance arising from fluid molecular interactions should be considered, as pointed out by Wang & Hadjiconstantinou (2019), how to quantify its effect on slip velocity remains unresolved. As shown in figure 2(*a*), the resistance for a fluid molecule moving forwards originates from two components, namely the solid-liquid energy barrier ΔE_{wf} and the fluid-fluid energy barrier ΔE_{ff} (Blake & De Coninck 2002; Zhao & Cheng 2017; Wang & Hadjiconstantinou 2019). Here, we will develop our slip model through modelling of ΔE_{wf} and ΔE_{ff}.

In our model, the molecular interactions between molecules are treated by the 12-6 LJ potential as in MD simulations (Thompson & Troian 1997; Martini *et al.* 2008*a*; Morciano *et al.* 2017), i.e.

$$\phi_{ij} = 4\epsilon_{ij}\left[\left(\frac{\sigma_{ij}}{r}\right)^{12} - \left(\frac{\sigma_{ij}}{r}\right)^{6}\right], \tag{3.7}$$

where ϵ_{ij} and σ_{ij} are the energy and length parameters, r is the distance between molecules, and the subscript i and j denote two interacting molecules. While the 12-6 LJ potential is widely adopted in MD simulations (Thompson & Troian 1997; Martini *et al.* 2008*a*,*b*; Falk *et al.* 2010; Bailey *et al.* 2017; Morciano *et al.* 2017), it is seldom used in the mesoscopic kinetic and macroscopic continuum models (Mashayak & Aluru 2012; Bhadauria *et al.* 2015; Shan *et al.* 2020). The effective radii of two different types of molecules is chosen at a position where repulsive interaction become pronounced. In addition, the energy parameter ϵ is related to the induced dipole interactions between two molecules. Therefore, the mixed energy and length parameters are determined by the Lorentz-Berthelot combination rule (Lorentz 1881; Berthelot 1898)

$$\sigma_{ij} = \frac{\sigma_i + \sigma_j}{2}, \quad \epsilon_{ij} = \sqrt{\epsilon_i \epsilon_j}. \tag{3.8}$$

Considering the 12-6 LJ fluid-solid interactions and the lattice structure of the solids, the fluid-solid energy barrier ΔE_{wf} can be expressed as

$$\Delta E_{wf} = a\epsilon_{wf}, \tag{3.9}$$

where a is a constant characterizing the strength of fluid-solid interactions. Although the relationship in (3.9) appeared in some studies (Wang & Zhao 2011; Wang & Hadjiconstantinou 2019), a full explanation of its physical meaning as well as its derivation is still missing. We include the detailed derivation and numerical validation in Appendix A.

Now we focus on modelling the effect of fluid molecular interaction on slip. The overall impact of surrounding fluid molecules on the slip of a molecule can be depicted by this term: $\exp[-\Delta E_{ff}/(k_B T)]$ (Wang & Hadjiconstantinou 2019). However, an explicit determination of ΔE_{ff} is difficult (Wang & Hadjiconstantinou 2019). Since ΔE_{ff} is related to fluid

molecules in both the interfacial and bulk regions, see figure 2(*a*), we propose the following transformation,

$$\frac{\Delta E_{ff}}{k_B T} \sim \frac{\epsilon_{wf}}{\epsilon_{ff}}. \tag{3.10}$$

It is noted that although the left term in (3.10) explicitly includes temperature T, the term $\Delta E_{ff}/(k_B T)$ can be regarded as independent of T. For the physical process of molecular slip, an empty site will be available in the flow direction when a fluid molecule moves forward. According to Glasstone *et al.* (1941), the work required to make such an empty site is equal to the energy of vaporization ΔE_{vap}, which can relate to ΔE_{ff} as

$$\Delta E_{vap} \sim \Delta E_{ff}. \tag{3.11}$$

As $\Delta E_{vap}/(k_B T) = b(v_m/v_f)^{1/3}$ (with b being the packing number, v_m being the molecular volume, and v_f being the molecular free volume; these parameters are negligibly affected by temperature) (Glasstone *et al.* 1941; Blake & De Coninck 2002), $\Delta E_{vap}/(k_B T)$ can be considered to be independent of temperature. Based on equation (3.11) and the physical process of molecular slip, (3.10) is a reasonable approximation to explicitly consider the effect of fluid molecular interaction on slip.

Considering both fluid-fluid and fluid-solid molecular interactions on slip, our MKT slip model can be written as

$$u_s = f_{wet}\delta\frac{2k_B T}{h}\exp\left(-\frac{a\epsilon_{wf}}{k_B T}\right)\sinh\left(\frac{\tau S\delta}{2k_B T}\right), \tag{3.12}$$

where f_{wet} is a wettability factor accounting for fluid molecular interactions on slip, which can be expressed as

$$f_{wet} = c_1 \exp\left(-c_2\frac{\epsilon_{wf}}{\epsilon_{ff}}\right). \tag{3.13}$$

where c_1 and c_2 are two fitting parameters depending on fluid and solid molecular properties.

The above equation (3.12) is an extended MKT slip model, which bridges the molecular scale to the continuum hydrodynamics. Compared to the previous MKT slip models, all the parameters of our model are straightforward to determine, which do not depend on flow geometries or operation conditions. For example, δ is the distance between adjacent potential wells, which is related to the arrangement of solid molecules, see figure 2(*b*); S is the effective area, which can be taken as the square of the average distance between fluid molecules in the first adsorption layer; f_{wet} needs to be calibrated once by MD simulation for a given fluid-solid system. Both fluid-solid and fluid molecular interactions on slip are considered. The fluid-solid energy barrier is modelled by equation (3.9), while the fluid-fluid energy barrier is modelled by the wettability factor f_{wet} in (3.13). According to Barrat & Bocquet (1999) and Śliwińska-Bartkowiak *et al.* (2014), the ratio $\epsilon_{wf}/\epsilon_{ff}$ is directly related to the wettability. This is physically reasonable since the distribution of fluid molecules under confinement is controlled by the wettability. The critical shear stress and the energy dissipation between adsorption layers are not taken into account in (3.12), but it is convenient to consider them if necessary as in Wang & Zhao (2011). Since all parameters can be straightforwardly determined, this extended MKT slip model can be employed as a boundary condition for a continuum model to determine slip velocity at the fluid-solid interface, which will be elaborated in § 4.

It is noted that the slip velocity (3.12) models the hopping of molecules in the first adsorption layer, which corresponds to the surface diffusion rate of adsorbed gas (Ruckenstein & Rajora 1983; Shu *et al.* 2017). This is important in many engineering applications, such

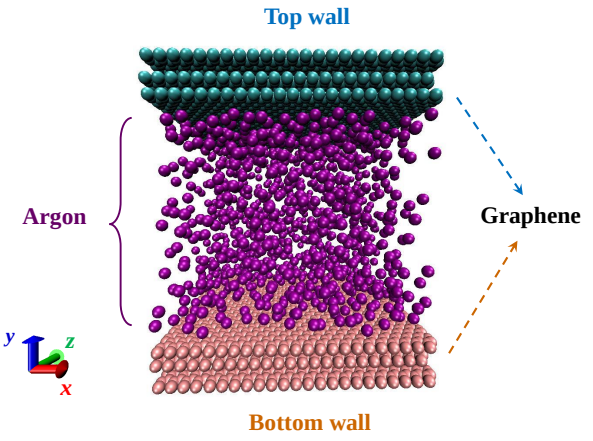

Figure 3: Schematic of the physical model in MD simulations

as shale gas and coal bed methane development, where adsorbed gas accounts for large proportion in low-permeability shales and coals (Wu *et al.* 2019; Zhang *et al.* 2019).

4. Results and discussion

Here, we apply the molecular-kinetic slip boundary condition (3.12) together with the generalised continuum model (2.4) and (2.5) to investigate nano-scale surface-confined Couette and Poiseuille flows. In Couette flows, the top and bottom plates move in the x and $-x$ directions at a speed of u_w, while a constant external force G_x is exerted on argon molecules in the x direction in Poiseuille flows. The details of determining slip velocities and slip lengths in Couette and Poiseuille flows are introduced in Appendices B and C, respectively.

Meanwhile, MD simulations using LAMMPS are conducted to validate the current continuum approach. In our non-equilibrium MD simulations, argon molecules are confined between two parallel graphite plates, as shown in figure 3. The 12-6 LJ potential is employed to model fluid-solid and fluid-fluid molecular interactions with a cut-off distance of 1.2 nm. The graphite molecules are fixed in our simulations. The system temperature is kept constant by implementing a Nosé-Hoover thermostat (Evans & Holian 1985). The periodic boundary condition is employed in the x and z directions, respectively. After reaching equilibrium, the simulations are run with a time step of 2 fs to a minimum duration of 20 ns.

In our continuum and MD simulations of the nano-confined flows, we employ the same input parameters to ensure quantitatively meaningful comparisons. Unless otherwise specified, the corresponding parameters are: (i) the characteristic length of the flow path is $H = 5$ nm, which is the distance between the first layer of solid molecules in the top and bottom plates; (ii) an isothermal process with the system temperature of $T = 313$ K is considered; (iii) the average density of the fluids is controlled at $\rho = 500$ kg/m^3; (iv) in the Couette flow, the top and bottom plates move with a speed of $u_w = 150$ m/s in the opposite directions; in the Poiseuille flow, the external force is set as $G_x = 0.0001$ kcal/(mol·Å); the plate velocity and the external force are chosen to ensure the flow in the linear flow regime, which means the slip length is not affected by the flow velocity; (v) the length and energy parameters of the solid and fluid as well as their masses are summarised in table 1.

Here, we examine the role of temperature, characteristic length of the flow domain,

	m, g/mol	σ, nm	ϵ, kcal/mol
Argon	39.95	0.3405	0.2378
Graphene	12.01	0.3390	0.0692

Table 1: Input parameters of argon (Barisik & Beskok 2011) and graphene (Suk & Aluru 2017) for the continuum and MD simulations.

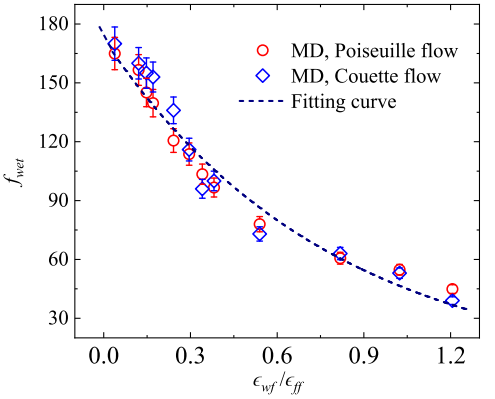

Figure 4: The dependency of wettability factor f_{wet} on energy parameters ratio $\epsilon_{wf}/\epsilon_{ff}$. The fitting curve is (3.13) with c_1 = 172.41 and c_2 = -1.28.

wettability, and density in slip dynamics. We also compare our slip model with the previous ones and establish a universal scaling law for the slip length.

4.1. *The wettability factor accounting for fluid molecular interactions*

In the present slip model (3.12), the effect of fluid molecular interaction on slip is reflected by the wettability factor f_{wet}, which represents the resistance a fluid molecule *feels* during slip exerted by its surrounding fluid molecules. By comparing slip velocities obtained from the slip model (3.12) and our MD simulations, the dependency of the wettability factor f_{wet} on energy parameters ratio $\epsilon_{wf}/\epsilon_{ff}$ can be obtained, as shown in figure 4. Here, the fitting parameter is only calibrated once for the argon and graphene surface by the MD simulation in both Couette and Poiseuille flows. The calibrated relationship will then be used for all the other cases where the same argon and graphene are used in the following discussion.

The wettability factor f_{wet} decreases rapidly with the energy parameters ratio $\epsilon_{wf}/\epsilon_{ff}$, indicating a larger fluid resistance on the slip of a molecule at stronger wettability conditions. As wettability increases, the fluid density becomes larger in the first adsorption layer, leaving less empty sites along the flow direction for an activated molecule to move forwards. Consequently, although the flow resistance from the bulk fluid becomes smaller, it is harder for a fluid molecule to slip. This also indicates that the flow resistance from the adsorbed fluid molecules is much larger than from the bulk ones.

4.2. *Effect of temperature on slip length*

The density and velocity profiles of the argon between the moving graphite plates are displayed in figure 5 at T = 253 K, T = 353 K, and T = 453 K, respectively. Here, to examine the effect of temperature, we keep all the parameters the same except for temperature. The

effect of other parameters (width, wettability and density) is also analyzed in this way in the following subsections.

As shown in figure 5, a strong adsorption layer forms at the fluid-solid interface followed by a second layer of weak adsorption due to the competition between the fluid-solid and fluid-fluid molecular interactions. As previously reported (Voronov *et al.* 2008; Ho *et al.* 2011), these epitaxial layering structures in the vicinity of solid surface dominate the slip dynamics at the fluid-solid interface at the nano-scale. Consequently, the boundary condition alone, no matter a hydrodynamic one or a molecular kinetic one, is not sufficient to describe the true slip dynamics, since the inhomogeneity of the fluid flow has to be considered by the governing equations (Hsu & Patankar 2010). Moreover, fluid adsorption is important in many engineering applications, e.g. unconventional shale gas production (Germanou *et al.* 2018; Zhang *et al.* 2019). Therefore, the required large-scale engineering simulations motivate us to develop a computationally efficient model to capture molecular-scale interactions and to accurately predict hydrodynamic behaviour at the system scale (Ho *et al.* 2019b).

Figure 5 also shows good agreement between our continuum and MD simulations considering the influence of temperature on the velocity profiles. Furthermore, from figure 5(*d*), we can see that the slip velocity increases with temperature, which is reasonable since the kinetic energy of the fluid molecules, which escape from the potential wells, is larger at a higher temperature. While the bulk fluid flow can be described by classical continuum models with slip boundary conditions, the detailed flow behavior of gas adsorption is completely ignored. However, the nanoscale confinement effect is more than a slip velocity at the solid surface, because the thickness of adsorption layers may not be negligibly small comparing to the flow dimension, which depends on the strength of interaction potentials between the surface and fluid molecules. Therefore, a slip velocity at the boundary is not sufficient to account for the nanoscale effect in an inhomogeneous system, which we would like to emphasise again.

The effect of temperature on velocity profiles of Poiseuille flows is shown in figure 6. Again, a good agreement between the continuum and the MD results is observed at different temperatures. Due to the large slip velocity in nano-graphene channels, the velocity distribution is plug-like, significantly enhancing the mass transfer efficiency in such structures.

4.3. *Effect of channel width on slip length*

The effect of channel width H on the slip length of Couette and Poiseuille flows is shown in figure 7 where H ranges from 2.0 nm to 13.0 nm. Previously, it was reported that the slip length L_s was independent of the channel width H (Cieplak *et al.* 2001) where the range of channel width was not specified. However, as shown in figure 7(*a*), the slip length does increase with the channel width rapidly in highly-confined Couette flows, while it decreases with the channel width H in Poiseuille flows. Keerthi *et al.* (2018) experimentally reported the helium transport driven by pressure through 2D nanochannels for different wall materials and observed that the slip length decreases with the channel width, which is consistent with our computational finding. However, helium has a smaller mass and weaker interactions with surface molecules, and the experiment was conducted in an ultra-rarefied condition with $Kn > 10^4$. Therefore, the observed enhancement effect in the experiment (Keerthi *et al.* 2018) is more significant than our simulations of dense argon flows with Kn close to 0.01. For both Couette and Poiseuille flows, when H becomes sufficiently large, the slip length plateaus, which is consistent with Kannam *et al.* (2013).

For comparison, the slip length obtained from the NS equation with the present slip model (3.12) is also included in figure 7, where the wettability factor is chosen to ensure the slip velocities for our continuum model and the NS equation are the same at $H = 5$ nm. The parameters such as viscosity and the effective area are evaluated at the average density

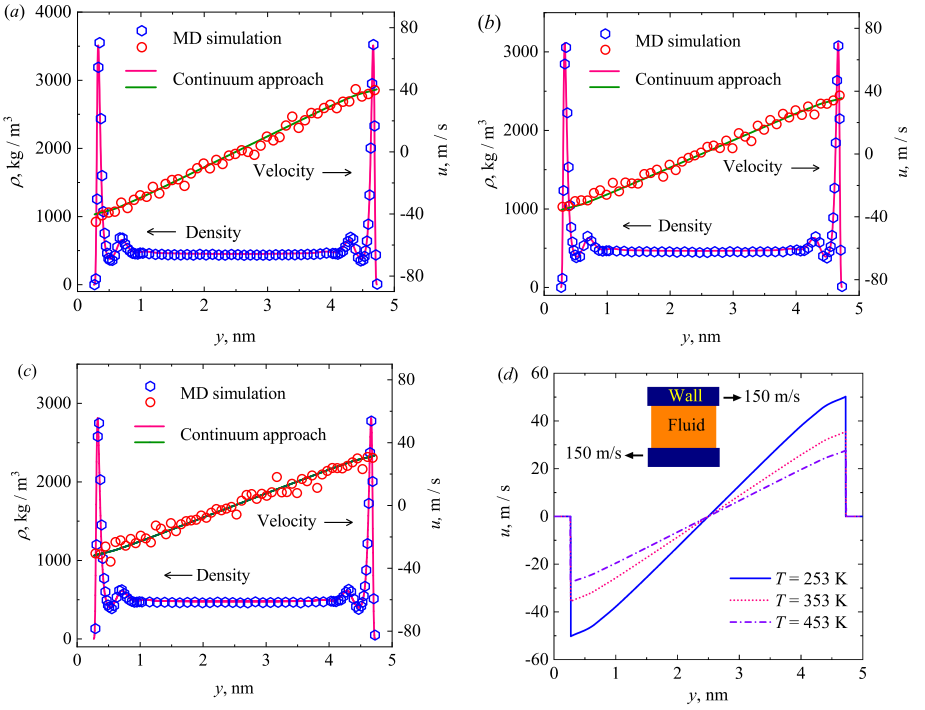

Figure 5: The comparison of cross-sectional density and velocity distributions between our continuum and MD simulations at (*a*) T = 253 K, (*b*) T = 353 K, and (*c*) T = 453 K, respectively; and (*d*) comparison of the velocity profiles obtained by the continuum model at different temperatures.

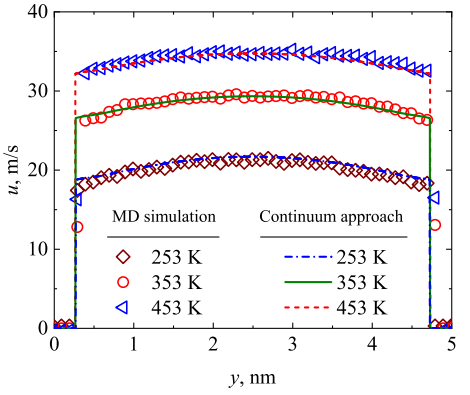

Figure 6: The effect of temperature on the velocity profiles of the Poiseuille flows.

ρ_{avg} = 500 kg/m^3. The NS model predicts that slip length does not depend on channel width, which is different from the finding of our continuum and MD simulations. This further proves that the a slip boundary condition alone cannot capture the slip dynamics accurately in small nano-channels, e.g., $H < 13$ nm in this study.

On the other hand, the normalised slip length, i.e. ratio of slip length to channel width L_s/H, decreases with the channel width in both Couette and Poiseuille flows, as shown in

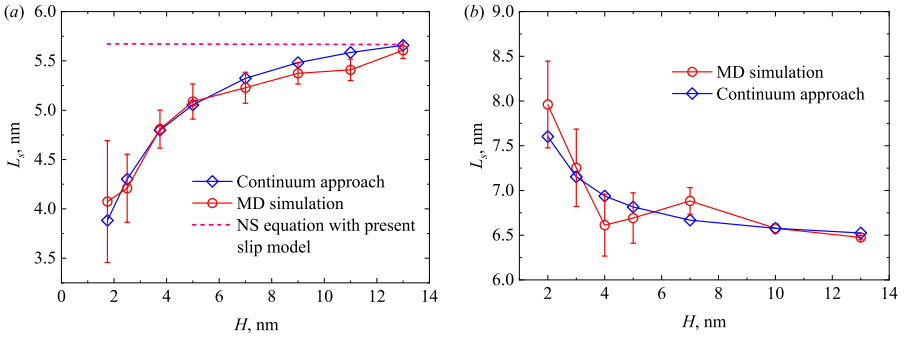

Figure 7: The effects of channel width H on the slip length, (a) the Couette flow, and (b) the Poiseuille flow.

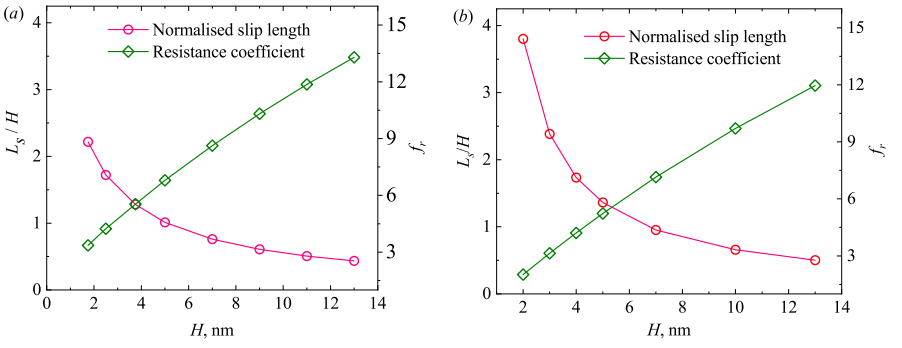

Figure 8: The effects of channel width H on the normalised slip length and the resistance coefficient, (a) the Couette flow, and (b) the Poiseuille flow.

figure 8. According to Cao *et al.* (2006), the flow resistance coefficient can be calculated by

$$f_r = \frac{48}{Re}\frac{1}{1+6\frac{L_s}{H}}, \tag{4.1}$$

where Re is the Reynolds number, and f is the resistance coefficient. As indicated by (4.1), the overall flow resistance is mainly controlled by the ratio L_s/H at a fixed Re. Figure 8 shows how the resistance coefficient varies with channel widths at $Re = 1$. Clearly, the flow resistance is smaller in the narrower nanochannels due to the larger L_s/H, i.e., the slip reduces the flow resistance in highly-confined nanochannels. Compared to a Couette flow, the flow resistance in a Poiseuille flow is smaller due to lager slip length at narrow nano-channels. This indicates that the nano-confinement effect on flow physics of Couette and Poiseuille flows is different.

4.4. *Effect of wettability on slip length*

The fluid-surface molecular interactions are key to understanding slip flow behaviours at the nano-scale. One of the main differences of our continuum model from the previous ones is that the fluid-fluid and fluid-solid molecular interactions are considered exactly the same as those in MD simulations. Here, the effect of molecular interactions, as reflected by ratio of the fluid-solid energy parameter to the fluid-fluid energy parameter, i.e. $\epsilon_{wf}/\epsilon_{ff}$, is investigated.

As shown in figure 9, the slip length decreases with $\epsilon_{wf}/\epsilon_{ff}$ via a power law relationship and tends to no-slip when this ratio is sufficiently large in both Couette and Poiseuille flows.

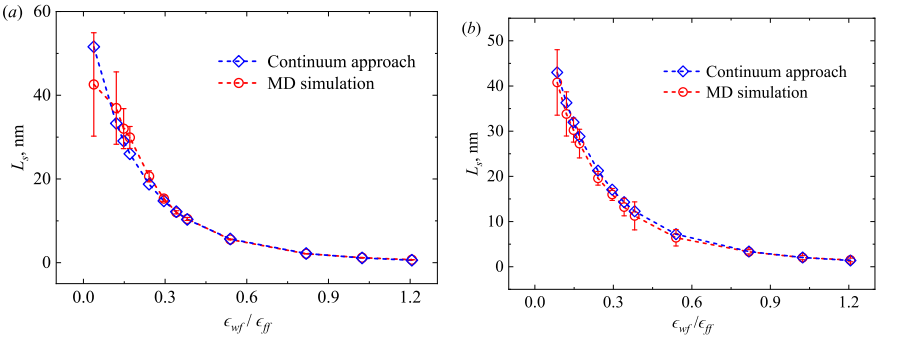

Figure 9: A comparison of the slip length predicted by our continuum and MD simulations at different wettability conditions, (*a*) the Couette flow, and (*b*) the Poiseuille flow.

Again, our continuum results agree well with the MD data. The strong interactions among fluid and solid molecules as well as the lack of empty sites along the flow direction resist the fluid molecules to slip over a solid substrate at larger $\epsilon_{wf}/\epsilon_{ff}$, while the solid surface becomes repulsive and the viscous resistance becomes smaller when the fluid-solid coupling becomes weaker, which prompts the fluid molecules to slip over the solid surface. This finding is also consistent with the results of previous MD simulations (Barrat & Bocquet 1999; Voronov *et al.* 2006).

4.5. *Effects of density on slip length*

It was reported that the slip length decreases with fluid density in the MD simulations (Koplik *et al.* 1989; Barrat & Bocquet 1999; Voronov *et al.* 2008), which is consistent with the kinetic theory for rarefied gas flows. However, it is shown by our continuum model that the slip length increases with density for large densities, as shown in figure 10.

We perform MD simulations for the Couette and Poiseuille flows to verify this new finding. Our results are shown in figure 10. In both types of flows, there are two distinct regimes I and II divided by the critical density marked by the vertical dashed line at $\rho = 400$ kg/m^3. For a dense fluid flow, the Kn is defined (Chapman & Cowling 1970) as

$$Kn = \frac{1}{\sqrt{2} n_{avg} \pi \sigma^2 \chi H}, \tag{4.2}$$

where n_{avg} is the average fluid number density. Using this definition, the Kn is approximately 0.046 in the system considered. Consequently, in the regime I, namely for $\rho < 400$ kg/m^3 ($Kn > 0.046$), the rarefaction effect is important, where the fluid-solid molecular interaction dominates. In this regime, the slip length increases as density decreases, which is consistent with the gas kinetic theory (Koplik *et al.* 1989; Barrat & Bocquet 1999; Voronov *et al.* 2008). In the regime II for $\rho > 400$ kg/m^3 ($Kn < 0.046$), the fluid becomes denser. In this regime, the average distance between fluid molecules is much smaller, and the fluid-fluid molecular interaction becomes non-negligible. The slip length in this regime is found to increase with the fluid density, which is contrary to the kinetic theory.

The above competing fluid-solid and fluid molecular interactions on the slip length L_s can be intuitively explained by the definition of the slip length. In (2.7), the slip velocity can be expressed as $u_s = \tau/\zeta = \eta\gamma/\zeta$ with ζ being the friction coefficient between the fluid and solid, and the slip length can consequently be expressed by two properties of the fluid-solid

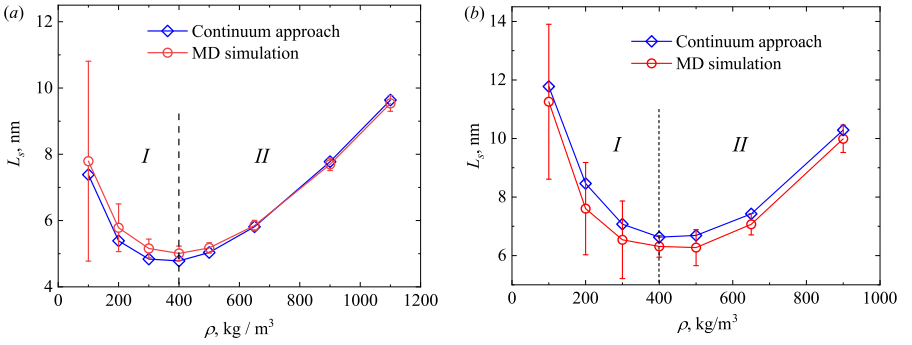

Figure 10: A comparison of the slip length dependence on density between the continuum and MD simulations, (*a*) the Couette flow, and (*b*) the Poiseuille flow.

system, namely

$$L_s = \frac{\eta}{\zeta}. \tag{4.3}$$

At different densities, the fluid viscosity η can be calculated by equation (2.3), while the friction coefficient ζ can be derived from the slip model (3.12), see Appendix D. The friction coefficient and viscosity can reflect the strength of fluid-solid and fluid-fluid molecular interactions, respectively. Although both parameters increase with density, the friction coefficient increases faster for small densities and more slowly for large densities, but the opposite is true for the viscosity, see figure 11. The competing effect between fluid-solid and fluid-fluid molecular interactions leads to slip length minimum analogous to the Knudsen minimum phenomenon in rarefied gas dynamics as shown in figure 11(*b*). So at small densities, the flow is dominated by fluid-solid interaction where the slip length decreases when the density increases. While at large densities, the flow is dominated by fluid molecular interactions where the slip length increases with density. Furthermore, the inflexion density is also at approximately $\rho = 425\text{kg/m}^3$, which is close to the continuum and MD simulation results presented in figure 10, supporting our explanation of the physical mechanism underlying the slip length minimum. It is noted that the slip length shown in figure 11 is higher than our continuum and MD simulation results presented in figure 10. This discrepancy arises from the fact that the effective area S in equation (D 3) is evaluated using the average density, while the density of the adsorbed gas should be used since the slip occurs at the adsorption layer in the immediate contact with the wall. With this correction, the predicted slip lengths are consistent.

The slip length minimum can also explained from an force balance perspective. In a Couette flow, for example, it is the friction force that drives the fluid layer adjacent to the plates to move first, and the bulk fluid will resist this movement through the viscous shear force. In the regime *II*, the fluid viscosity becomes large as density increases such that the friction force at the fluid-solid interface is not sufficient to overcome the viscous shear force in the central bulk region at a larger shear rate (i.e. a smaller slip length). Consequently, the shear rate will decrease to reduce the viscous shear force to establish a steady Couette flow, which explains the increasing slip length with density in this regime. This phenomenon can also be observed at different fluid-solid coupling strengths, as shown in figure 10(*b*).

4.6. *A scaling law for the slip length minimum*

As we can see from figures 10 and 11(*b*), the regime *I*, where the fluid-solid interaction dominates the flow, transits to the regime *II*, where the fluid molecular interaction is more

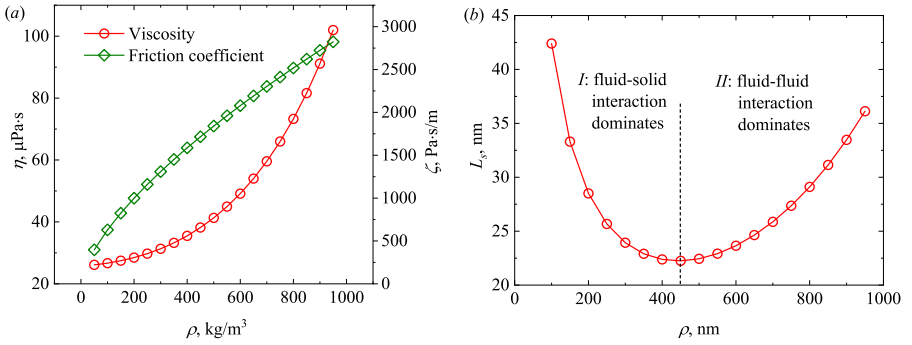

Figure 11: (*a*) the variation of viscosity and friction coefficient with density, and (*b*) the competing effect of the fluid-solid and fluid-fluid molecular interactions on slip length.

important, at nearly the same inflection density. As discussed above, the non-monotonicity of the slip length dependency on density reflects the competition between the fluid-solid and fluid molecular interactions, which can be characterised by the friction coefficient and the viscosity, respectively. This slip length minimum is interestingly analogous to the Knudsen minimum (Sheng *et al.* 2020).

Meanwhile, as indicated by the generalised hydrodynamic model (2.1) and (2.4), wall potential ϕ_w and fluid intermolecular potential ϕ_m as well as the system temperature T play crucial roles in the strongly inhomogeneous systems. To quantify the effect of these factors, the parameter $\prod$ is devised as (Guo *et al.* 2006*a*)

$$\prod = \frac{1}{H-2\iota}\int_{\iota}^{H-\iota}\frac{\phi_w+\phi_m}{k_BT}dy \approx \frac{\epsilon_{ff}}{k_BT}\left(b_1\frac{\sigma}{H}\frac{\epsilon_{wf}}{\epsilon_{ff}}+b_2n\sigma^3\right), \tag{4.4}$$

where ι is the distance between the first fluid layer to the solid, and b_1 and b_2 are two constants related to the wall potential and the fluid intermolecular potential, respectively. Consequently, a typical nanoscale dense fluid system can be characterised by the four non-dimensional parameters, i.e., the reduced temperature $T_r = k_BT/\epsilon_{ff}$, the confinement factor H/σ, the energy ratio $\epsilon_{wf}/\epsilon_{ff}$, and the reduced fluid density $n\sigma^3$.

Inspired by equation (4.4), we propose the following universal scaling law for non-dimensional slip length as

$$L_s^n = \frac{L_s}{\sigma}\frac{H}{\sigma}\left(\frac{\epsilon_{wf}}{\epsilon_{ff}}\right)^{\beta}\frac{\epsilon_{ff}}{k_BT}\frac{\eta}{\eta_0}Kn, \tag{4.5}$$

where β is a constant for a given solid and fluid system. Here, the ratio $\epsilon_{wf}/\epsilon_{ff}$ reflects the competition between the fluid-wall and fluid molecular interactions, and the ratio $\epsilon_{ff}/(k_BT)$ capitulates the competition between the fluid internal potential energy and kinetic energy. The denseness effect is characterised by the viscosity ratio between the dense fluid and the corresponding dilute one, i.e., η/η_0, and the rarefaction effect is illustrated by the Knudsen number Kn. Using this scaling law, the relationship between the non-dimensional slip length L_s^n and the reduced density $\hat{n} = n\sigma^3$ in different systems is shown in figure 12, where all the data almost collapse into a single line. This confirms our statement that the non-monotonicity of slip length on density is a result of the competition between the fluid-solid and fluid molecular interactions, analogous to the Knudsen minimum. At low densities, the slip length decreases when the density increases, while it increases with the density linearly at high densities, regardless of the fluid-solid coupling strength, the system temperature and dimension.

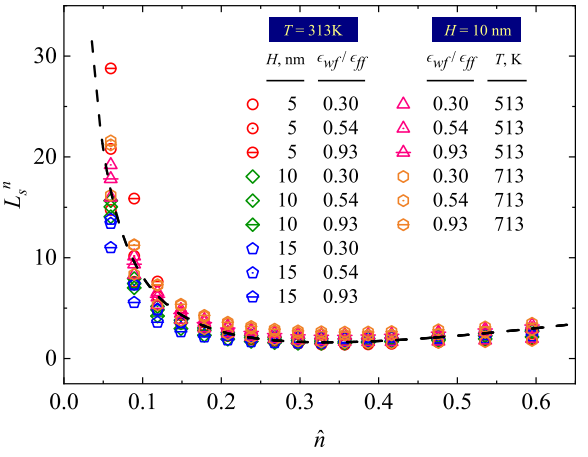

Figure 12: A universal scaling law of slip length considering the effects of density, fluid-solid coupling strength, channel width, and system temperature.

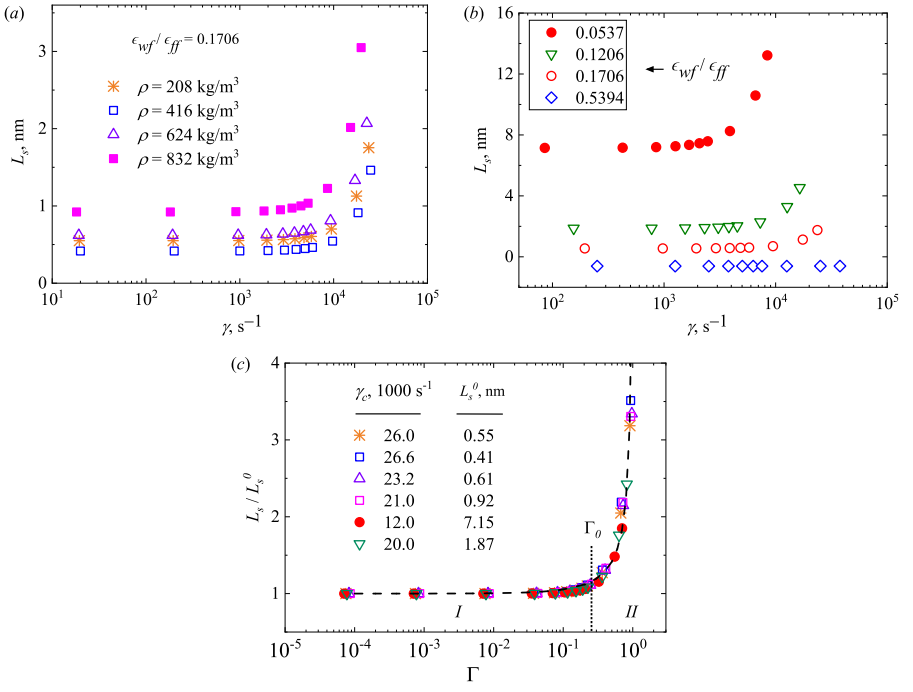

Figure 13: Dependency of the slip length on (*a*) density; (*b*) fluid-solid coupling strength; and (*c*) comparison between our continuum model (symbols) and the general scaling law (4.6) of Thompson & Troian (1997) (dash line).

4.7. *Slip length dependency on shear rate*

The pioneering work of Thompson & Troian (1997) reported that the Navier slip boundary condition is only applicable at low shear rates, and the slip length increases rapidly with γ at high shear rates (Thompson & Troian 1997). Based on their MD simulation results, a general

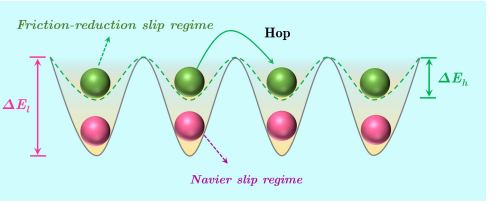

Figure 14: The fluid slip length at low and high shear rates

scaling law for the slip length was proposed as

$$L_s = L_s^0(1-\Gamma)^{-0.5}, \tag{4.6}$$

where L_s^0 is the limiting slip length at low shear rates, Γ is the ratio of the shear rate γ to the critical shear rate γ_c.

The present continuum model allows us to simulate a wide range of nano-scale confined flows with different densities, temperatures, fluid-solid coupling strengths, shear rates and flow geometries to check the validity of the above scaling law and to unravel the underlying mechanisms. Our simulation results are shown in figure 13. The slip length dependency on density and fluid-solid coupling strength can be clearly observed. The slip length is nearly constant at low shear rates and increases rapidly after the critical shear rate γ_c. The results also suggest that the critical shear rate is not affected by the density, but increases with the increasing fluid-solid coupling strength. It is noted that a stick slip, where the slip length is negative, is found in at the strong fluid-solid coupling strength in figure 13(*b*).

In figure 13(*c*), the dash line is the results of the scaling law (4.6) obtained from the MD simulations (Thompson & Troian 1997), which are in excellent agreement with our results. As shown in figure 13(*c*), two slip flow regimes are divided by the non-dimensional shear rate $\Gamma = \Gamma_0$ as indicated by the vertical dash line. With $\Gamma < \Gamma_0$, it is the linear Navier slip flow regime (*I*), in which the slip length increases linearly with the shear rate, namely the so-called linear response regime. When $\Gamma > \Gamma_0$, the friction-reduction slip flow regime starts. In this regime (*II*), the friction coefficient decreases with the shear rate. Our continuum model is able to capture this unique molecular-scale slip characteristics, which further confirms the validity of our model. So the present continuum mode is well-suited for large-scale simulations beyond the reach of MD simulations.

At a fluid-solid interface, the microscopic friction coefficient ζ is defined as the ratio of viscosity to slip length, namely equation (4.3). For Newtonian fluids, the viscosity η is independent of shear rate (Thompson & Troian 1997). As the slip length increases, the friction coefficient decreases with the shear rate. This reduction of the friction coefficient can be explained by the landscape of energy corrugation. There are energy corrugations over the wall surface due to the lattice structure of solids, see figure 14. At a low shear rate, there is sufficient time for fluid molecules to occupy the low energy sites and remain in a stable state, as shown in figure 14 of the Navier slip flow regime. In this regime (*I*), the fluid molecules (in red) need to overcome ΔE_l to hop from one site to another. As the shear rate increases, the speed of fluid molecules at the interface also increases. When the fluid moves fast enough, fluid molecules do not invaginate themselves into the lower potential energy levels, but rather skim over the substrate (Martini *et al.* 2008*a*), exhibiting a smaller energy barrier depth ΔE_h. When the shear rate, i.e. the fluid moving speed is sufficiently large, the energy barrier depth tends to zero, namely $\Delta E \to 0$. In this case, the solid-fluid interface becomes frictionless, and the slip tends to be infinite (Wu *et al.* 2017), i.e. $L_s \to +\infty$.

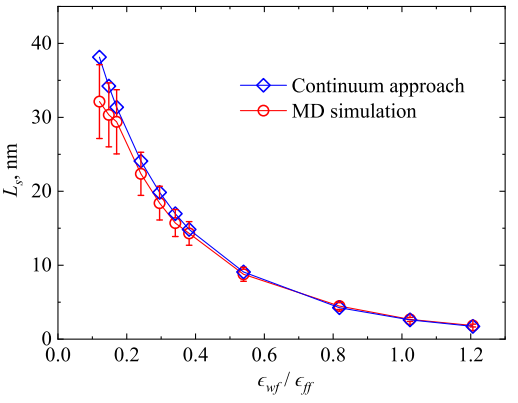

Figure 15: Using the continuum approach to simulate the slip flows of ρ = 800 kg/m^3, T = 353 K, H = 6 nm over a wide range of fluid-solid coupling strengths.

4.8. *Model analysis*

Here, we apply the continuum model (2.1 and 3.12) to simulate the slip flows of ρ = 800 kg/m^3, T = 353 K, H = 6 nm using the wettability factor f_{wet} relationship in figure 4 which is calibrated at ρ = 500 kg/m^3, T = 313 K and H = 5 nm. The results of the slip flows over a wide range of fluid-solid coupling strengths are presented in figure 15. The corresponding MD simulations are also conducted which show good agreement with the continuum results, see figure 15. As the wettability weakens, the continuum results gradually deviate from the MD data. Considering the uncertainties in MD simulations and the large slip in the simulated system for low wettability, the relative difference is still not significant. Therefore, the new boundary condition (3.12) can help the present continuum model to accurately simulate slip flows, which is computationally efficient to enable practical engineering simulations. Even if the energy parameter of carbon molecules ϵ_w is changed, the boundary condition still holds as long as the array of surface molecules remain unchanged, which further indicates the applicability of the present continuum model for nanoscale confined flows.

4.9. *A comparison with other slip models*

The MKT slip model (3.4) proposed by Wang & Zhao (2011) reduces to (3.3), which is proposed by Glasstone *et al.* (1941), if the shear stress is low and the critical shear stress is neglegible. In our study, the simulated cases are in the linear flow regime and there is no critical shear stress observed. Therefore, we compare our model with the Glasstone MKT model described by equation (3.3). Meanwhile, the commonly employed second-order slip boundary condition for the NS equation is also included for comparison,which is

$$u_s^{app} - u_w = \pm C_1 \lambda \left(\frac{\partial u}{\partial n}\right)_s - C_2 \lambda^2 \left(\frac{\partial^2 u}{\partial n^2}\right)_s, \tag{4.7}$$

where C_1 and C_2 are the first- and second-order slip coefficients, which are taken as C_1 = 1.0 and C_2 = 0.5 in our study (Chapman & Cowling 1970). Combining the 2nd order slip boundary condition with the Stokes equation, the slip velocity can be calculated as

$$u_s^{app} = -\frac{H^2}{2\eta}\frac{\mathrm{d}p}{\mathrm{d}x}(C_1 Kn + 2C_2 Kn^2). \tag{4.8}$$

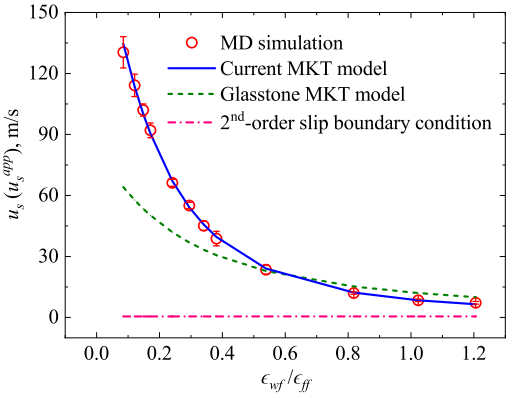

Figure 16: Model comparison for slip velocity under different wettability, where the MD results serve as the benchmark solution.

Here, we note that only the apparent slip velocity can be calculated from the 2nd order slip boundary condition, while a micro slip velocity can only be calculated from MKT slip models.

The comparison of different models are shown in figure 16, where the MD data serve as the benchmark solution. The Glasstone model (3.3) fails to capture the slip dynamics for different wettability, while the results of the current model are in excellent agreement with the MD data. Since the Kn is independent of the wettability, the slip velocity from the 2nd-order slip boundary condition is constant, which is much smaller than the other predictions, especially for weak wettability. Therefore, the 2nd-order slip boundary condition is not applicable for strongly inhomogeneous nano-scale flows.

4.10. *Navier Stokes equation with the current slip model*

As discussed above, a slip boundary condition alone cannot accurately capture the flow dynamics in nano-scale systems. Here, with a slip velocity known *in priori*, the velocity distributions obtained from the present continuum model and the NS equation are compared for two different wettabilities. Again, the MD simulation results serve as the benchmark solution.

In the NS equation, the molecule size is not considered. So the depletion area, arising from the finite size of solid and fluid molecules, as well as the possibly strong repulsion between the solid and fluid molecules, is neglected in the NS equation. Therefore, the physical channel width (defined in figure 1 as H) should be kept equal for equivalent comparison, which means the effective channel width in the NS model is increased by the thickness of two depletion areas at the channel walls. From the computational perspective, the width of depletion area cannot be determined in the NS model, and the physical channel width should be chosen.

In figure 17, the velocity distributions across the channel are compared, where the velocity $\hat{u}$ is defined as

$$\hat{u} = u - u_s, \tag{4.9}$$

where u_s is the slip velocity. As shown in the figure, the velocity distribution across the channel depends on wettability. The fluid flows fast at the weak fluid-solid coupling, i.e., small $\epsilon_{wf}/\epsilon_{ff}$. In contrast, the effect of fluid-solid coupling is not considered in the NS equation and the simulated velocity is not affected by wettability, which deviates from the MD data, especially for large wettability, see figure 17. This indicates that a slip boundary condition alone cannot capture slip dynamics in strongly inhomogeneous nano-scale systems,

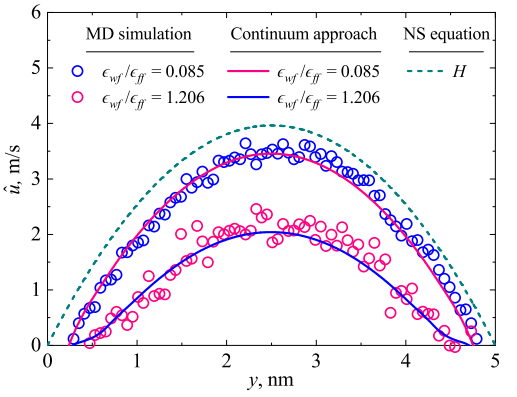

Figure 17: A comparison of the present continuum model with the NS solutions. The MD results serve as the benchmark solution.

where the fluid-fluid and fluid-solid molecular interactions need to be considered by the corresponding governing equations.

5. Conclusions

In this work, the molecular kinetic boundary condition is developed to allow the generalised hydrodynamic model to probe the molecular-scale slip behaviours in nanoscale channels. In this continuum model, the molecular-scale slip characteristics are captured using the projected 12-6 LJ and 10-4-3 LJ potentials for the fluid-fluid and fluid-solid molecular interactions, which are consistent with those used in MD simulations. Therefore, the surface influence is also considered in the momentum equation as a mean-field force. A slip boundary condition alone is not sufficient to capture the molecular-scale fluid dynamics.

Slip length is found to decrease with density when the density is below the critical value, and increases with density at larger densities. This non-intuitive behaviour is a consequence of the force balance between surface friction and viscous force, reflecting competing fluid-solid and fluid molecular interactions. A universal scaling law for the slip length which captures the slip length minimum is proposed. The shear-rate dependent slip length is reproduced by the present continuum model, which shows the two distinctive slip regimes, i.e. the Navier slip regime at low shear rates, and the friction-reduction regime at high shear rates. The influence of temperature, density, channel width, and fluid/surface coupling strength (i.e. wettability) on the slip length are also investigated. Interestingly, the slip length is found to increase with the channel width in a Couette flow, and to decrease in a Poiseuille flow before it becomes independent of the channel width when the channel width is beyond a critical value. The results show that the proposed slip boundary condition is applicable to different thermodynamic states and fluid-solid systems once the wettability factor f_{wet} is calibrated.

The present continuum model provides an efficient and accurate method to simulate strongly inhomogeneous confined fluid flows at the nano-scale, which can describe both molecular-scale and macroscopic fluid dynamics. In comparison with MD, which is computationally costly, this continuum model can be used for large-scale practical simulations.

Acknowledgement

This work is supported by the National Natural Science Foundation of China (Grant No. 51836003 and No. 12002130). And funding support from the UK's Engineering and Physical

Sciences Research Council under Grant No. EP/R041938/1 is also acknowledged. Valuable advice from Prof. Fengchao Wang of the University of Science and Technology of China about their MKT slip model is highly appreciated.

Declaration of interests

The authors declare no competing interests.

Appendix A. Modelling of fluid-solid energy barrier

Fluid-solid molecular interaction is responsible to fluid adsorption and slip in the vicinity of the wall. Here, we attempt to develop a simplified model for the fluid-solid interaction, which can retain the essential physics. We employ a structureless plate to depict the role of fluid-solid interaction in the formation of adsorption layers, since adsorption is hardly affected by the lattice structure of the solid. As the fluid and solid molecules interact via 12-6 LJ potential (3.7), the total potential exerted by all the solid molecules on a fluid molecule can be calculated by an integration of the 12-6 potential over the whole solid surface, which is

$$\begin{aligned} E_{wf}(y) &= 4n_w\epsilon_{wf}\int_0^{2\pi}\mathrm{d}\omega\int_0^{+\infty}\left[\frac{\sigma_{wf}^{12}}{(r^2+y^2)^6}-\frac{\sigma_{wf}^{6}}{(r^2+y^3)^3}\right]r\,\mathrm{d}r, \\ &= 2n_w\pi\epsilon_{wf}\sigma_{wf}^2\left[\frac{2}{5}\left(\frac{\sigma_{wf}}{y}\right)^{10}-\left(\frac{\sigma_{wf}}{y}\right)^{4}\right]. \end{aligned} \tag{A 1}$$

This is the so-called 10-4 LJ potential, acting upon a fluid molecule adjacent to the solid surface by all the wall molecules. We can see that solid-fluid molecular interaction depends on the perpendicular distance between the fluid molecule and the planar wall. This surface force is strongly repulsive when the distance is small, and becomes attractive when the fluid molecule moves away from the surface. This type of wall potential has been extensively used in the previous studies (Bitsanis *et al.* 1987; Guo *et al.* 2006*a*), and produced the results in good agreement with the MD simulations. Under the influence of this potential, the fluid molecules would preferentially occupy the most stable positions, namely the locations with the lowest energy potential. Let $\partial E_{wf}/\partial y = 0$, the location of equilibrium sites with the lowest potential can be found at $y = \sigma_{wf}$.

According to the MD studies (Thompson & Troian 1997; Lichter *et al.* 2007; Martini *et al.* 2008*a*,*b*), there should be some energy undulations in the flow direction due to the lattice structure of solid surfaces. The fluid density varies tangentially along the solid surface because fluid molecules preferentially occupy sites of lower energy over the solid surface. To encapsulate this mechanism, a small perturbation is implemented in the 10-4 LJ potential to generate energy corrugations along the flow direction. According to the previous studies (Martini *et al.* 2008*a*,*b*; Hsu & Patankar 2010), assuming that the energy corrugation satisfies a sine function with the amplitude of e, which is small comparing to the total energy potential, the potential distribution over the solid surface can then be expressed as

$$E_{wf}(x,y) = E_{wf}(y)\left[1+e\sin\left(\frac{2\pi}{\delta}x\right)\right]. \tag{A 2}$$

Here, we conduct numerical simulations to evaluate accuracy of the perturbation described by a sinusoidal function in (A 2). All the 12-6 fluid-solid interaction pairs between the solid and fluid molecules are summed numerically to compare with the analytical solution.

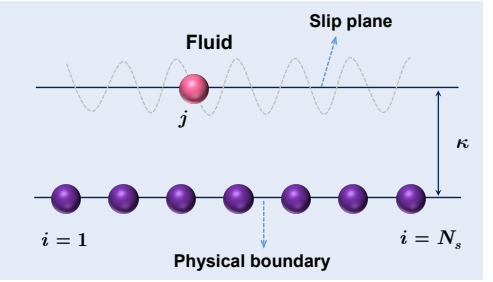

Figure 18: A schematic of numerical summation of the fluid-solid potential on the slip plane

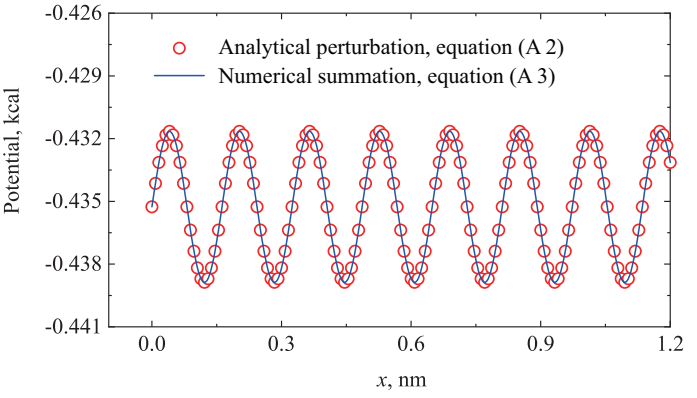

Figure 19: The energy corrugation over a solid surface: validation of the analytical perturbation given by (A 2).

Assuming there are N_s solid molecules, the total potential exerted by all solid molecules on the position j in the slip plane (see figure 18) can be calculated by summation as

$$\hat{E}_{wf}(j) = \sum_{i=1}^{N_s} \phi_{ij}, \tag{A 3}$$

where $\hat{E}_{wf}(j)$ is the potential that a fluid molecules *feels* at an arbitrary position j on the slip plane. The potential distribution along the slip plane can be obtained numerically, as shown in figure 19. The energy corrugation is well described by (A 2), and the perturbation is small comparing to the local average potential, i.e. $e \ll E_{wf}(\kappa)$, where κ is the normal distance between the equilibrium sites and the solid surface, as shown in figure 2. At a constant height over the solid surface, the fluid molecules would experience a fluctuating potential as they pass over the discrete solid atoms (Steele 1973). Therefore, this inhomogeneous potential in the surface of the first fluid layer dominates the slip dynamics at the boundary. In the bulk region, this energy corrugation can be ignored, since it decreases very rapidly (exponentially) with its distance to the wall.

According to (A 2), for an energy corrugation with the amplitude of e, the energy barrier depth ΔE can be expressed as

$$\Delta E = 2eE_{wf}(\kappa). \tag{A 4}$$

This demonstrates a linear relationship between the energy barrier depth ΔE and the energy parameter ϵ_{wf} for a pair of solid-fluid molecules. In order to further prove this point, we

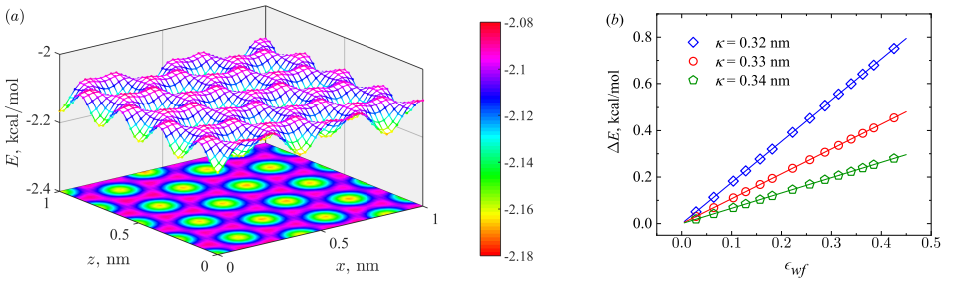

Figure 20: The energy corrugation over a graphite solid at the equilibrium surface (a) and the relationship between the energy barrier depth ΔE and the energy parameter ϵ_{wf} fitted by (3.9) with a = 1.77, 1.07, and 0.66 for κ = 0.32 nm, 0.33 nm, and 0.34 nm, respectively (b).

take a two-dimensional graphene surface as an example. The total potential distribution in a surface at a distance $\kappa = 0.34$ nm from the solid is determined numerically by a superposition of each solid-fluid molecular interaction pair. This energy corrugation is clearly shown in figure 20(a). In figure 20(b), the linear relationship between ΔE and ϵ_{wf} in surfaces at different distances from the solid (κ = 0.32 nm, 0.33 nm and 0.34 nm) is confirmed by the linear fitting between ΔE and ϵ_{wf}, i.e. the equation (3.9).

For the multiple solid layers, the fluid-solid interactions can be described by the 10-4-3 LJ potential, also known as the Steele potential (Steele 1973), which can be written as

$$E_{wf}(y) = 2n_w\pi\epsilon_{wf}\sigma_{wf}^2 L\left[\frac{2}{5}\left(\frac{\sigma_{wf}}{y}\right)^{10} - \left(\frac{\sigma_{wf}}{y}\right)^{4} - \frac{\sigma_{wf}^4}{3L(y+0.61L)^3}\right], \tag{A 5}$$

where L is the distance between adjacent solid plates. The relationship (3.9) still holds for the 10-4-3 LJ potential, which can be proved similarly as the 10-4 LJ potential.

Appendix B. Slip velocity and slip length in Couette flows

In a Couette flow, the shear stress $\tau = \eta(y)\gamma(y)$ should be a constant according to (2.5). Integrating (2.5) over the channel, the shear stress can be obtained as

$$\tau = \frac{2(u_w - u_s)}{\int_0^H \frac{1}{\eta(y)}\,\mathrm{d}y}. \tag{B 1}$$

Combining (3.12) and (B 1), the slip velocity u_s can be solved, after which the velocity across the channel can be obtained by

$$u|_{y=y_0} = u_w - u_s - \int_{y_0}^{H} \frac{\tau}{\eta(y)}\,\mathrm{d}y. \tag{B 2}$$

For a Couette flow, the equation (2.7) for calculating the slip length reduces to

$$L_s = \frac{u_w}{\gamma} - \frac{H}{2}. \tag{B 3}$$

Appendix C. Slip velocity and slip length in Poiseuille flows

In a nano-scale confined Poiseuille flow, the shear stress is not explicitly specified. Integrating the equation (2.6) and combining the symmetric condition $\gamma(y = H/2) = 0$, the shear stress

distribution can be obtained as

$$\tau|_{y=y_0} = \left(\eta \frac{du}{dy}\right)\Big|_{y=y_0} = G\int_{y_0}^{H/2} n(y)\,\mathrm{d}y, \tag{C 1}$$

from which we can see that the stress is related to the external force, the density distribution and the position. The stress at the bottom solid-fluid interface can be expressed as

$$\tau|_{y=0} = \left(\eta \frac{du}{dy}\right)\Big|_{y=0} = G\int_{0}^{H/2} n(y)\,\mathrm{d}y = \frac{Gn_{avg}H}{2}. \tag{C 2}$$

Taking this stress into (3.12), the slip velocity can be determined. The velocity distribution can then be obtained by integrating (C 1)

$$u|_{y=0} = \int_0^{y_0} \frac{\tau}{\eta}\Big|_{y=0}\,\mathrm{d}y + u_s. \tag{C 3}$$

For the Poiseuille flow, the slip length can be characterised by the apparent and intrinsic mass flow rate as

$$L_s = \frac{(Q_{app}/Q_{ins} - 1)H}{6}, \tag{C 4}$$

where Q_{app} and Q_{ins} are the apparent and intrinsic mass flow rates, respectively. The intrinsic mass flow rate refers to flow satisfying Poiseuille law with a no-slip boundary condition, which is calculated by

$$Q_{ins} = -\frac{\rho H^3 w}{12\eta_{avg}}\nabla p, \tag{C 5}$$

where w is the width of nano-channel in the z direction, and ∇p is the pressure gradient related to external force by $-\nabla p = Gn$.

The apparent mass flow rate considers the effect of fluid density inhomogeneities and slip at the fluid-solid interface, which can be evaluated by

$$Q_{app} = wH\int_0^H \rho(y)u(y)\,\mathrm{d}y. \tag{C 6}$$

Appendix D. The derivation of the friction coefficient

The derivation is divided into two regimes depending on the value of $\frac{\tau S\delta}{2k_BT}$. At small $\frac{\tau S\delta}{2k_BT}$, the hyperbolic function can be approximated by

$$\sinh\left(\frac{\tau S\delta}{2k_BT}\right) \approx \frac{\tau S\delta}{2k_BT}. \tag{D 1}$$

Consequently, the slip model (3.12) can be rewritten as

$$\tau = u_s \frac{h}{f_{wet}\delta^2 S}\exp\left(\frac{a\epsilon_{wf}}{k_BT}\right). \tag{D 2}$$

According to the relationship $\tau = \zeta u_s$, the friction coefficient at small shear stress can be obtained as

$$\zeta = \frac{h}{f_{wet}\delta^2 S}\exp\left(\frac{a\epsilon_{wf}}{k_BT}\right). \tag{D 3}$$

802 At large $\frac{\tau S\delta}{2k_BT}$, the hyperbolic function can be approximated by

803 $$\sinh\left(\frac{\tau S\delta}{2k_BT}\right) \approx \frac{1}{2}\exp\left(\frac{\tau S\delta}{2k_BT}\right), \tag{D 4}$$

804 and the slip model (3.12) can be rewritten as

805 $$\tau = \frac{2k_BT}{S\delta}\ln\left[u_s\frac{h}{k_BTf_{wet}\delta}\exp\left(\frac{a\epsilon_{wf}}{k_BT}\right)\right]. \tag{D 5}$$

806 Consequently, the friction coefficient at large stress can be evaluated by

807 $$\zeta = \frac{2k_BT}{S\delta u_s}\ln\left[u_s\frac{h}{k_BTf_{wet}\delta}\exp\left(\frac{a\epsilon_{wf}}{k_BT}\right)\right], \tag{D 6}$$

808 from which we can see that the friction coefficient depends on not only the system properties,
809 but also the slip velocity at high shear stress. This corresponds to the friction reduction
810 regime at high shear rate.

REFERENCES

811 Bailey, N. Y., Hibberd, S. & Power, H. 2017 Dynamics of a small gap gas lubricated bearing with navier
812 slip boundary conditions. *J. Fluid Mech.* **818**, 68–99.
813 Barisik, M. & Beskok, A. 2011 Equilibrium molecular dynamics studies on nanoscale-confined fluids.
814 *Microfluid. Nanofluid.* **11** (3), 269–282.
815 Barrat, J. L. & Bocquet, L. 1999 Large slip effect at a nonwetting fluid-solid interface. *Phys. Rev. Lett.*
816 **82** (23), 4671–4674.
817 Berthelot, Daniel 1898 Sur le mélange des gaz. *Compt. Rendus* **126**, 1703–1706.
818 Bhadauria, R., Sanghi, T. & Aluru, N. R. 2015 Interfacial friction based quasi-continuum hydrodynamical
819 model for nanofluidic transport of water. *J. Chem. Phys.* **143** (17), 174702.
820 Bitrián, V. & Principe, J. 2018 Driving mechanisms and streamwise homogeneity in molecular dynamics
821 simulations of nanochannel flows. *Phy. Rev. Fluids* **3** (1), 014202.
822 Bitsanis, I., Magda, J. J., Tirrell, M. & Davis, H. T. 1987 Molecular dynamics of flow in micropores. *J.*
823 *Chem. Phys.* **87** (3), 1733–1750.
824 Bitsanis, I., Vanderlick, T. K., Tirrell, M. & Davis, H. T. 1988 A tractable molecular theory of flow in
825 strongly inhomogeneous fluids. *J. Chem. Phys.* **89** (5), 3152–3162.
826 Blake, T. D. & De Coninck, J. 2002 The influence of solid–liquid interactions on dynamic wetting. *Adv.*
827 *Colloid Interfac.* **96** (1-3), 21–36.
828 Cai, J. C., Zhang, Z. E., Wei, W., Guo, D. M., Li, S. & Zhao, P. Q. 2019 The critical factors for permeability-
829 formation factor relation in reservoir rocks: Pore-throat ratio, tortuosity and connectivity. *Energy* **188**,
830 116051.
831 Cao, B. Y., Chen, M. & Guo, Z. Y. 2006 Liquid flow in surface-nanostructured channels studied by
832 molecular dynamics simulation. *Phys. Rev. E* **74** (6 Pt 2), 066311.
833 Chapman, S & Cowling, T. G. 1970 *The mathematical theory of non-uniform gases*. Cambridge, England:
834 Cambridge University Press.
835 Cieplak, M., Koplik, J. & Banavar, J. R. 2001 Boundary conditions at a fluid-solid interface. *Phys. Rev.*
836 *Lett.* **86** (5), 803–806.
837 Dalton, B. A., Glavatskiy, K. S., Daivis, P. J. & Todd, B. D. 2015 Nonlocal response functions
838 for predicting shear flow of strongly inhomogeneous fluids. ii. sinusoidally driven shear and
839 multisinusoidal inhomogeneity. *Phys. Rev. E* **92** (1), 012108.
840 Davis, T. H. 1987 Kinetic theory of flow in strongly inhomogeneous fluids. *Chem. Eng. Commun.* **58** (1-6),
841 413–430.
842 De Coninck, J. & Blake, T. D. 2008 Wetting and molecular dynamics simulations of simple liquids. *Annu.*
843 *Rev. Mater. Res.* **38**, 1–22.
844 Evans, D. J. & Holian, B. L. 1985 The nose-hoover thermostat. *J. Chem. Phys.* **83** (8), 4069–4074.
845 Falk, K., Sedlmeier, F., Joly, L., Netz, R. R. & Bocquet, L. 2010 Molecular origin of fast water transport in

carbon nanotube membranes: superlubricity versus curvature dependent friction. *Nano. Lett.* **10** (10), 4067–4073.

Germanou, L., Ho, M. T., Zhang, Y. H. & Wu, L. 2018 Intrinsic and apparent gas permeability of heterogeneous and anisotropic ultra-tight porous media. *J. Natural Gas Sci. Eng.* **60**, 271–283.

Glasstone, S., Laidler, K. J.s & Eyring, H. 1941 The theory of rate processes: The kinetics of chemical reactions, viscosity, diffusion and electrochemical phenomena. *Tech. Rep.*. McGraw-Hill Book Company.

Granick, S., Zhu, Y. X. & Lee, H. 2003 Slippery questions about complex fluids flowing past solids. *Nat. Mater.* **2** (4), 221–227.

Guo, Z. L., Zhao, T. S. & Shi, Y. 2005 Simple kinetic model for fluid flows in the nanometer scale. *Phys. Rev. E* **71** (3), 035301.

Guo, Z. L., Zhao, T. S. & Shi, Yong 2006*a* Generalized hydrodynamic model for fluid flows: From nanoscale to macroscale. *Phys. Fluids* **18** (6), 067107.

Guo, Z. L., Zhao, T. S., Xu, C. & Shi, Y. 2006*b* Simulation of fluid flows in the nanometer: kinetic approach and molecular dynamic simulation. *Intl. J. Comput. Fluid. D.* **20** (6), 361–367.

Heiranian, M. & Aluru, N. R. 2020 Nanofluidic transport theory with enhancement factors approaching one. *ACS Nano* **14** (1), 272–281.

Henot, M., Grzelka, M., Zhang, J., Mariot, S., Antoniuk, I., Drockenmuller, E., Leger, L. & Restagno, F. 2018 Temperature-controlled slip of polymer melts on ideal substrates. *Phys. Rev. Lett.* **121** (17), 177802.

Ho, M. T., Li, J., Su, W., Wu, L., Borg, M., Li, Z. & Zhang, Y. H. 2020 Rarefied flow separation in microchannel with bends. *J. Fluid Mech.* **901**, A26.

Ho, M. T., Zhu, L., Wu, L., Wang, P., Guo, Z., Li, Z. & Zhang, Y. H. 2019b A multi-level parallel solver for rarefied gas flows in porous media. *Comput. Phys. Commun.* **234**, 14–25.

Ho, M. T., Zhu, L., Wu, L., Wang, P., Guo, Z., Ma, J. & Zhang, Y. H. 2019a Pore-scale simulations of rarefied gas flows in ultra-tight porous media. *Fuel* **249**, 341–351.

Ho, T. A., Papavassiliou, D. V., Lee, L. L. & Striolo, A. 2011 Liquid water can slip on a hydrophilic surface. *P. Natl. Acad. Sci. USA* **108** (39), 16170–16175.

Hocking, L. M. 1976 A moving fluid interface on a rough surface. *J. Fluid Mech.* **76** (4), 801–817.

Holt, J. K., Park, H. G., Wang, Y. M., Stadermann, M., Artyukhin, A. B., Grigoropoulos, C. P., Noy, A. & Bakajin, O. 2006 Fast mass transport through sub-2-nanometer carbon nanotubes. *Science* **312** (5776), 1034–1037.

Hsu, H. Y. & Patankar, N. A. 2010 A continuum approach to reproduce molecular-scale slip behaviour. *J. Fluid Mech.* **645**, 59–80.

Kannam, S. K., Todd, B. D., Hansen, J. S. & Daivis, P. J. 2013 How fast does water flow in carbon nanotubes? *J. Chem. Phys.* **138** (9), 094701.

Kavokine, N., Netz, R. R. & Bocquet, L. 2021 Fluids at the nanoscale: From continuum to subcontinuum transport. *Annu. Rev. Fluid Mech.* **53**, 377–410.

Keerthi, A., Geim, A. K., Janardanan, A, Rooney, A. P., Esfandiar, A., Hu, S., Dar, S. A., Grigorieva, I. V., Haigh, S. J., Wang, F. C. & others 2018 Ballistic molecular transport through two-dimensional channels. *Nature* **558** (7710), 420–424.

Koplik, J., Banavar, J. R. & Willemsen, J. F. 1989 Molecular dynamics of fluid flow at solid surfaces. *Phys. Fluids* **1** (5), 781–794.

Lauga, E. & Stone, H. A. 2003 Effective slip in pressure-driven stokes flow. *J. Fluid Mech.* **489**, 55–77.

Lichter, S., Martini, A., Snurr, R. Q. & Wang, Q. 2007 Liquid slip in nanoscale channels as a rate process. *Phys. Rev. Lett.* **98** (22), 226001.

Lorentz, H. A. 1881 Ueber die anwendung des satzes vom virial in der kinetischen theorie der gase. *Anna. Phys.* **248** (1), 127–136.

Ma, L., Gaisinskaya-Kipnis, A., Kampf, N. & Klein, J. 2015 Origins of hydration lubrication. *Nat. Commun.* **6**, 6060.

Ma, M. D., Shen, L. M., Sheridan, J., Liu, J. Z., Chen, C. & Zheng, Q. S. 2011 Friction of water slipping in carbon nanotubes. *Phys. Rev. E* **83** (3), 036316.

Martini, A., Hsu, H. Y., Patankar, N. A. & Lichter, S. 2008*a* Slip at high shear rates. *Phys. Rev. Lett.* **100** (20), 206001.

Martini, A., Roxin, A., Snurr, R. Q., Wang, Q. & Lichter, S. 2008*b* Molecular mechanisms of liquid slip. *J. Fluid Mech.* **600**, 257–269.

Mashayak, S. Y. & Aluru, N. R. 2012 Coarse-grained potential model for structural prediction of confined water. *J. Chem. Theory Comput.* **8** (5), 1828–1840.

Morciano, M., Fasano, M., Nold, A., Braga, C., Yatsyshin, P., Sibley, D. N., Goddard, B. D., Chiavazzo, E., Asinari, P. & Kalliadasis, S. 2017 Nonequilibrium molecular dynamics simulations of nanoconfined fluids at solid-liquid interfaces. *J. Chem. Phys.* **146** (24), 244507.

Nott, P. R. 2011 Boundary conditions at a rigid wall for rough granular gases. *J. Fluid Mech.* **678**, 179–202.

Patashinski, A. Z., Ratner, M. A., Orlik, R. & Mitus, A. C. 2019 Nanofluidic manifestations of structure in liquids: A toy model. *J. Phys. Chem. C* **123** (27), 16787–16795.

Pozhar, L. A. & Gubbins, K. E. 1993 Transport theory of dense, strongly inhomogeneous fluids. *J. Chem. Phys.* **99** (11), 8970–8996.

Priezjev, N. V. & Troian, S. M. 2006 Influence of periodic wall roughness on the slip behaviour at liquid/solid interfaces: molecular-scale simulations versus continuum predictions. *J. Fluid Mech.* **554** (1), 25–46.

Richardson, S. 1973 On the no-slip boundary condition. *J. Fluid Mech.* **59** (4), 707–719.

Ruckenstein, E. & Rajora, P. 1983 On the no-slip boundary condition of hydrodynamics. *J. Colloid Interf. Sci.* **96** (2), 488–491.

Secchi, E., Marbach, S., Nigues, A., Stein, D., Siria, A. & Bocquet, L. 2016 Massive radius-dependent flow slippage in carbon nanotubes. *Nature* **537** (7619), 210–213.

Shan, B. C., Wang, P., Zhang, Y. H. & Guo, Z. L. 2020 Discrete unified gas kinetic scheme for all knudsen number flows. iv. strongly inhomogeneous fluids. *Phys. Rev. E* **101** (4-1), 043303.

Sheng, Q., Gibelli, L., Li, J., K Borg, M. K. & Zhang, Y. H. 2020 Dense gas flow simulations in ultra-tight confinement. *Phys. Fluids* **32** (9), 544–550.

Sholl, D. S. & Johnson, J. K. 2006 Materials science. making high-flux membranes with carbon nanotubes. *Science* **312** (5776), 1003–1004.

Shu, J. J., Teo, J. B.M. & Chan, W. K. 2017 Fluid velocity slip and temperature jump at a solid surface. *Appl. Mech. Rev.* **69** (2).

Śliwińska-Bartkowiak, M., Sterczyńska, A., Long, Y. & Gubbins, K. E. 2014 Influence of microroughness on the wetting properties of nano-porous silica matrices. *Mol. Phys.* **112** (17), 2365–2371.

Sochi, T. 2011 Slip at fluid-solid interface. *Polym. Rev.* **51** (4), 309–340.

Steele, W. A. 1973 The physical interaction of gases with crystalline solids: I. gas-solid energies and properties of isolated adsorbed atoms. *Surf. Sci.* **36** (1), 317–352.

Suk, M. E. & Aluru, N. R. 2017 Modeling water flow through carbon nanotube membranes with entrance/exit effects. *Nanosc. Microsc. Therm.* **21** (4), 247–262.

Thompson, P. A. & Troian, S. M. 1997 A general boundary condition for liquid flow at solid surfaces. *Nature* **389** (6649), 360–362.

Urbakh, M., Klafter, J., Gourdon, D. & Israelachvili, J. 2004 The nonlinear nature of friction. *Nature* **430** (6999), 525–528.

Vanderlick, T. K., Scriven, L. E. & Davis, H. T. 1989 Molecular theories of confined fluids. *J. Chem. Phys.* **90** (4), 2422–2436.

Voronov, R. S., Papavassiliou, D. V. & Lee, L. L. 2006 Boundary slip and wetting properties of interfaces: correlation of the contact angle with the slip length. *J. Chem. Phys.* **124** (20), 204701.

Voronov, R. S., Papavassiliou, D. V. & Lee, L. L. 2008 Review of fluid slip over superhydrophobic surfaces and its dependence on the contact angle. *Ind. Eng. Chem. Res.* **47** (8), 2455–2477.

Wang, F. C. & Zhao, Y. P. 2011 Slip boundary conditions based on molecular kinetic theory: The critical shear stress and the energy dissipation at the liquid–solid interface. *Soft Matter* **7** (18), 8628–8634.

Wang, G. J. & Hadjiconstantinou, N. G. 2019 Universal molecular-kinetic scaling relation for slip of a simple fluid at a solid boundary. *Phy. Rev. Fluids* **4** (6), 064201.

Wu, K., Chen, Z., Li, J., Li, X., Xu, J. & Dong, X. 2017 Wettability effect on nanoconfined water flow. *P. Natl. Acad. Sci. USA* **114** (13), 3358–3363.

Wu, L., Liu, H. H., Reese, J. M. & Zhang, Y. H. 2016 Non-equilibrium dynamics of dense gas under tight confinement. *J. Fluid Mech.* **794**, 252–266.

Wu, Y.Q., Tahmasebi, P., Lin, C. Y., Zahid, M. A., Dong, C. M., Golab, A. N. & Ren, L. H. 2019 A comprehensive study on geometric, topological and fractal characterizations of pore systems in low-permeability reservoirs based on sem, micp, nmr, and x-ray ct experiments. *Mar. Petrol. Geol.* **103**, 12–28.

958 Yang, F. Q. 2020 Slip boundary condition for viscous flow over solid surfaces. *Chem. Eng. Commun.*
959 **197** (4), 092003.
960 Yao, L., S., Sanjayan, Song, J. L., C., Colin R., Carmalt, C. J. & Parkin, I. P. 2015 Robust self-cleaning
961 surfaces that function when exposed to either air or oil. *Science* **347** (6226), 1132–1135.
962 Yuan, Q. Z. & Zhao, Y. P. 2013 Multiscale dynamic wetting of a droplet on a lyophilic pillar-arrayed
963 surface. *J. Fluid Mech.* **716**, 171–188.
964 Zampogna, G. A., Magnaudet, J. & Bottaro, A. 2018 Generalized slip condition over rough surfaces. *J.*
965 *Fluid Mech.* **858**, 407–436.
966 Zhang, L. H., Shan, B. C., Zhao, Y. L. & Guo, Z. L. 2019 Review of micro seepage mechanisms in shale
967 gas reservoirs. *Intl. J. Heat Mass Transfer* **139**, 144–179.
968 Zhao, L. & Cheng, J. T. 2017 Analyzing the molecular kinetics of water spreading on hydrophobic surfaces
969 via molecular dynamics simulation. *Sci. Rep.* **7** (1), 1–12.
970 Zhu, Y. & Granick, S. 2001 Rate-dependent slip of newtonian liquid at smooth surfaces. *Phys. Rev. Lett.*
971 **87** (9), 096105.